



# Panoptic SwiftNet: Pyramidal Fusion for Real-time Panoptic Segmentation

Josip Šarić<sup>a,\*\*</sup>, Marin Oršić<sup>b</sup>, Siniša Šegvić<sup>a</sup>

<sup>a</sup> University of Zagreb, Faculty of Electrical Engineering and Computing, Zagreb, Croatia

<sup>b</sup> Microblink, Zagreb, Croatia

Article history:

panoptic segmentation, real-time processing, image parsing, deep learning, computer vision

## ABSTRACT

Dense panoptic prediction is a key ingredient in many existing applications such as autonomous driving, automated warehouses or agri-robotics. However, most of these applications leverage the recovered dense semantics as an input to visual closed-loop control. Hence, practical deployments require real-time inference over large input resolutions on embedded hardware. These requirements call for computationally efficient approaches which deliver high accuracy with limited computational resources. We propose to achieve this goal by trading-off backbone capacity for multi-scale feature extraction. In comparison with contemporaneous approaches to panoptic segmentation, the main novelties of our method are scale-equivariant feature extraction and cross-scale upsampling through pyramidal fusion. Our best model achieves 55.9% PQ on Cityscapes val at 60 FPS on full resolution 2MPx images and RTX3090 with FP16 Tensor RT optimization.

© 2022 Elsevier Ltd. All rights reserved.

## 1. Introduction and related work

Panoptic segmentation [1] recently emerged as one of the most important recognition tasks in computer vision. It combines object detection and semantic segmentation in a single task. The goal is to assign a semantic class and instance index to each image pixel. Panoptic segmentation finds its applications in a wide variety of fields such as autonomous driving, automated warehouses or smart agriculture. Many of these applications require real-time inference in order to support timely decisions. However, most of the current state of the art does not meet that requirement [2, 3, 4, 5, 6, 7, 8]. State-of-the-art panoptic approaches [2, 8, 5, 7] are usually based on high capacity backbones in order to ensure a large receptive field which is required for accurate recognition in large-resolution images. Some of them are based on instance segmentation approaches and therefore require complex postprocessing in order to fuse instance-level detections with pixel-level classification [2, 8].

Different than all previous approaches to panoptic segmentation, we propose to leverage multiresolution processing [9] in order to increase the receptive field and decrease pressure onto the backbone capacity through scale equivariance [10]. In sim-

ple words, processing images on coarse resolutions may provide a more appropriate view at large objects. A mix of features from different scales is both semantically rich and positionally accurate. This allows our model to achieve 55.9% PQ at 60 FPS on full resolution Cityscapes val when evaluating with a RTX 3090 GPU and FP16 Tensor RT optimization.

This work contributes the first study of pyramidal fusion for panoptic segmentation. We point out that panoptic performance can be significantly improved by leveraging a boundary aware offset loss. Our models outperform generalization performance of the previous state-of-the-art in efficient panoptic segmentation [3] while offering 60% faster inference.

Pyramidal fusion was introduced for semantic segmentation [9]. Further work [11] showed that it outperforms spatial pyramid pooling [12] with respect to the effective receptive field. Our work explores its suitability for panoptic segmentation.

Early work on joint semantic and instance segmentation evaluated model performance separately, on both of the two tasks [13, 14]. The field gained much attention with the definition of a unified task called panoptic segmentation and the corresponding metric — panoptic quality [1]. This offered an easy transition towards the new task due to straight-forward upgrade of the annotations: panoptic segmentation labels can be acquired by combining existing semantic and instance segmentation labels.

<sup>\*\*</sup>Corresponding author. E-mail address: [josip.saric@fer.hr](mailto:josip.saric@fer.hr)

Thus, many popular recognition datasets [15, 16, 17] were able to release panoptic segmentation benchmarks in short amount of time, which facilitated further research.

Most of the recent panoptic segmentation methods fall under one of the two categories: box-based (or top-down) and box-free (also known as: bottom-up) methods. Box-based methods predict the bounding box of the instance and the corresponding segmentation mask. Usually, semantic segmentation of stuff classes is predicted by a parallel branch of the model. The two branches have to be fused in order to produce panoptic predictions. Panoptic feature pyramid network [2] is one of the first approaches for panoptic segmentation. It extends the popular Mask R-CNN [18] with a semantic segmentation branch dedicated to the stuff classes. Their fusion module favors instance predictions in pixels where both branches predict a valid class. Concurrent work [8] followed a similar extension idea, but proposed a different postprocessing step. UPSNet [8] stacks all instance segmentation masks and stuff segmentation maps and applies the softmax to determine the instance index and semantic class in each pixel. EfficientPS [19] is based on the EfficientNet backbone with custom upsampling and panoptic fusion. Although, it improves the efficiency, its inference speed (6 FPS) is still far from real time.

Box-free methods do not detect instances through bounding box regression. Most of these methods rely on grouping pixels into instances during a post-processing stage. Deeplab [4] extends a typical semantic segmentation architecture [20] with a class-agnostic instance segmentation branch. This branch detects five keypoints per object instance and groups pixels according to multiple range-dependent maps of offset vectors. Panoptic Deeplab [3] opts for a simpler instance segmentation branch. This branch outputs a single heat-map of object centers and a dense map of offset vectors which associate each thing pixel with the centroid of the corresponding instance. Panoptic FCN [21] also detects object centers, however they aggregate instance pixels through regressed per-instance kernels. MaxDeeplab [22] encodes a fixed number ( $N = 128$ ) of mask embeddings by a transformer module starting from a learnable initial representation. In parallel, a standard convolutional module produces per-pixel embeddings. The two modules share information through cross-attention. The panoptic masks are obtained with dot-product and softmax over all masks. This approach seems inappropriate for real time processing of large images since it requires parallel evaluation of the convolutional network and the transformer.

## 2. Method

Our panoptic segmentation approach inherits pyramidal SwiftNet architecture [11]. Unlike [3], we use the same decoder for semantic segmentation, and center and offset regression, and attach all three heads to the same latent representation at  $4\times$  subsampled resolution. The regressed centers and offsets enable class-agnostic instance segmentation as in [3]. Panoptic segmentation maps are recovered by fusing information from all three prediction heads.

### 2.1. Upsampling multi-scale features through pyramidal fusion

We start from a ResNet-18 backbone [23] and apply it to a three-level image pyramid consisting of images at the original,  $2\times$  and  $4\times$  downsampled resolution. Such organization only marginally increases the computational effort, but significantly increases the model ability to recognize large objects in high resolution images. The proposed upsampling path effectively increases the receptive field through multi-scale feature blending which we denote as pyramidal fusion. Pyramidal fusion proved beneficial for the semantic segmentation performance [11] and we hypothesise that this might be the case for panoptic segmentation as well. In order to properly determine the instance centroid, the model needs to have a look at the whole instance. This is hard to achieve when targeting real-time inference on large images since computational complexity is linear in number of pixels. We conjecture that pyramidal fusion is an efficient way to increase the receptive field and enrich the features with global context.

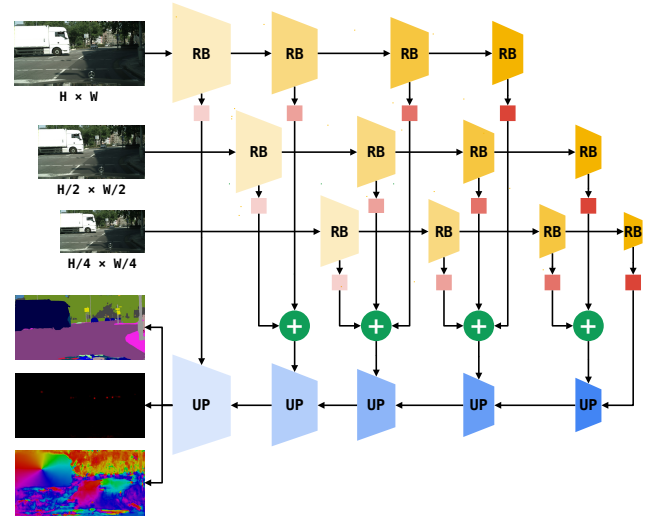


Fig. 1. Panoptic SwiftNet with three-way multi-scale feature extraction and pyramidal fusion. Yellow trapezoids denote residual blocks (RB). Red squares represent a  $1 \times 1$  convolutional projection. Blue trapezoids represent upsampling modules. Modules with the same color share parameters.

Figure 1 illustrates the proposed architecture. Yellow trapezoids represent residual blocks of a typical backbone which operate on  $4\times$ ,  $8\times$ ,  $16\times$  and  $32\times$  subsampled resolutions. The trapezoid color indicates feature sharing: the same instance of the backbone is applied to each of the input images. Thus our architecture complements scale-equivariant feature extraction with scale-aware upsampling. Skip connections from the residual blocks are projected with a single  $1 \times 1$  convolution (red squares) in order to match the number of channels in the upsampling path. Features from different pyramid levels are combined with elementwise addition (green circles). The upsampling path consists of five upsampling modules. Each module fuses features coming from the backbone via the skip connections and features from the previous upsampling stage. The fusion is performed through elementwise addition and a single  $3 \times 3$  convolution. Subsequently, the fused features are upsampled by bilinear interpolation. The last upsampling module outputs a

feature tensor which is four times subsampled w.r.t. to the input resolution. This feature tensor represents a shared input to the three prediction heads which output: semantic segmentation, center heatmap and offset vectors. Each head consists of a single  $1 \times 1$  convolution and  $4\times$  bilinear upsampling. Such design of the prediction heads is significantly faster than [3], because it avoids slow depthwise separable convolution with large kernel size  $k = 5$  on large resolution tensor. For brevity, we refer to BN-ReLU-CONV blocks as convolutions.

Different from the original semantic segmentation model, the upsampling path now needs to provide features which can discriminate instances. This is somewhat opposite to semantic segmentation which requires a unified representation for all instances of the same semantic class. Thus, we increase the upsampling capacity from 128 to 256 channels.

Our design differs from the previous work which advocates separate upsampling paths for semantic and instance specific predictions [3]. Our preliminary validation showed that mixed learning signals can improve panoptic performance when there is enough upsampling capacity.

## 2.2. Boundary-Aware Offset Loss

Regression of offset centers requires large prediction changes at instance boundaries. Accurate prediction in such pixels should distinguish between two neighboring instances. A displacement of only one pixel must make a distinction between two completely different instance centers. We conjecture that such abrupt changes require a lot of capacity.

Hence, we propose to prioritize the pixels at instance boundaries by learning offset regression through boundary-aware loss. We divide each instance into four regions according to the distance from the boundary. Each of the four regions is assigned a different weight factor. The largest weight factor is assigned to the regions which are closest to the border. The weights diminish as we go towards the interior of the instance. Consequently, we formulate the boundary-aware offset loss as follows:

$$\mathcal{L}_{BAOL} = \frac{1}{H \cdot W} \sum_{i,j}^{H,W} w_{i,j} \cdot |O_{i,j} - O_{i,j}^{GT}|, \quad w_{i,j} \in \{1, 2, 4, 8\} \quad (1)$$

## 2.3. The compound training loss

The model is trained with the compound loss consisting of three components. Our semantic segmentation loss  $\mathcal{L}_{SEM}$  is expressed as the usual per-pixel cross entropy. In Cityscapes experiments we additionally use hard-pixel mining and compute loss only in top 20% of pixels with the largest loss. The center regression loss  $\mathcal{L}_{CEN}$  corresponds to the L2 loss between the predicted centers heatmap and the ground truth heatmap. The offset loss  $\mathcal{L}_{BAOL}$  corresponds to the weighted L1 loss as described in (1). The three losses are modulated with the corresponding factors  $\lambda$  as follows:

$$\mathcal{L} = \lambda_{SEM} \cdot \mathcal{L}_{SEM} + \lambda_{CEN} \cdot \mathcal{L}_{CEN} + \lambda_{BAOL} \cdot \mathcal{L}_{BAOL} \quad (2)$$

Figure 2 shows ground truth labels for a single training example on Cityscapes. The semantic segmentation ground-truth labels are the same as for the semantic segmentation task (top-left). Ground-truth offsets point towards the respective instance

centers. Notice abrupt changes at instance-to-instance boundaries (top-right). The instance-center heatmap is crafted by Gaussian convolution ( $\sigma = 10$ ) of a binary image where ones correspond to instance centers (bottom-left). We craft the offset-weight ground-truth image by thresholding the distance transform with respect to instance boundaries. Note that pixels at stuff classes do not contribute to the offset loss since the corresponding weights are set to zero (bottom-right).

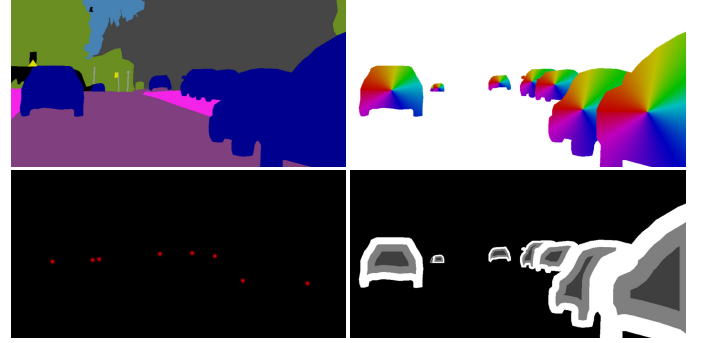


Fig. 2. Ground-truth labels for panoptic swiftnet training: semantic segmentation (top left), offset vectors (top right), heatmap for instance centers (bottom left), and weights for boundary-aware offset loss (bottom right).

## 2.4. Recovering panoptic predictions

We recover panoptic predictions through postprocessing of the three model outputs. First, a discrete set of instance centers is recovered by non-maximal suppression of the centers heatmap. Second, each thing pixel is assigned the closest instance center by taking into account the corresponding displacement from the offset map. Third, each instance is assigned a semantic class by taking arg-max over instance-specific semantic histograms. This voting process presents an opportunity to improve the original semantic predictions, as demonstrated in Figure 4 (right). Finally, the panoptic map is constructed by associating instance indices from step 2 and smoothed semantic indices from step 3.

We greatly improve the execution speed of our Python implementation by providing custom CUDA modules for steps 3 and 4. Still, our preliminary experiments on an embedded platform (Jetson AGX) indicate that postprocessing requires approximately the same amount of time as the inference of a model optimized with Tensor RT. This shows that further work is required in order to improve integration of Tensor RT models with custom CUDA kernels.

## 3. Experiments

We consider pyramid fusion models based on ResNet-18 [23] and DenseNet-121 [24]. We evaluate panoptic quality (PQ) [1] of our models on two road driving datasets with high resolution images: Cityscapes [15] and Mapillary Vistas [17]. We also evaluate on the COCO dataset [16] which gathers a very large number of images from personal collections. We also present experiments on semantic and instance segmentation tasks, and

**Table 1. Panoptic segmentation performance on Cityscapes val. The three sections correspond to top-down methods based on Mask R-CNN (top), bottom up methods (middle), and our methods based on pyramidal fusion (bottom). FPS denotes frames per second from PyTorch and Python. FPS\* denotes frames per second with FP16 TensorRT optimization. † — denotes our measurements.**

Model	PQ	AP	mIoU	FPS	FPS*	GPU
PanopticFPN-RN101 [2]	58.1	33.0	75.7	-	-	-
UPSNNet [8]	59.3	33.3	75.2	4.2	-	GTX 1080Ti
SeamLess-RN50 [5]	60.9	33.3	74.9	6.7	-	V100
RTPS-RN50 [7]	58.8	29.0	77.0	10.1	30.3	V100
DeeperLab-WMNv2 [4]	52.2	-	-	4.0	-	V100
PDL-MNv3 [3]	55.4	-	-	15.9	-	V100
PDL-MNv2 [3]	55.1	23.3	75.8	17.8†	42.2†	RTX3090
PSN-RN18 (ours)	55.9	26.1	77.2	<b>28.6</b>	<b>61.7</b>	RTX3090
PSN-DN121 (ours)	59.2	28.5	78.6	13.7	29.1	RTX3090

show the corresponding performance in terms of mean intersection over union (mIoU) and average precision (AP). We measure the inference speed of our models on different GPUs with and without TensorRT optimization.

### 3.1. Cityscapes

The Cityscapes dataset contains 2975 training, 500 validation and 1525 test images. All images are densely labeled. We train the models for 90000 iterations with ADAM optimizer on  $1024 \times 2048$  crops with batch size 8. This can be carried out on 2 GPUs each with 20GiB of RAM. We augment the crops through horizontal flipping and random scaling with factor between 0.5 and 2.0. We decay the learning rate from  $5 \cdot 10^{-5}$  to  $10^{-7}$  with a polynomial scheduler.

Table 1 compares our accuracy and inference speed with other methods from the literature. Our Panoptic SwiftNet model based on ResNet-18 achieves competitive accuracy with respect to models with more capacity, while being significantly faster. In comparison with Panoptic Deeplab [3] based on MobileNet v2, we observe that our method is more accurate in all three subtasks and also faster for 61% when measured in same runtime environment. We observe that methods based on Mask R-CNN [5, 2] achieve poor inference speed and uncompetitive semantic segmentation accuracy despite having larger backbone capacity.

Table 2 compares pyramidal fusion with spatial pyramid pooling [12, 25] as alternatives for providing global context. We train three separate models with 1, 2, and 3 levels of pyramidal fusion. None of these models contain any kind of pyramid

pooling module. We observe that spatial pyramid pooling improves AP and mIoU for almost 4 percentage points (cf. rows 1 and 2). This indicates that standard models are unable to capture global context due to undersized receptive field. This is likely exacerbated by the fact that we initialize with parameters obtained by training on  $224 \times 224$  ImageNet images. However, two-level pyramidal fusion outperforms the SPP model across all metrics. Three-level pyramid fusion achieves further improvements by outperforming the two-level model across all metrics. Furthermore, PYRx3 outperforms PYRx2 for 1pp PQ, 2.8pp AP and 1.1pp mIoU.

Table 3 explores the upper performance bounds w.r.t. particular model outputs. These experiments indicate that semantic segmentation represents the most important challenge towards accurate panoptic segmentation. Perfect semantic segmentation improves panoptic quality for roughly 20 points. However, we believe that rapid progress in semantic segmentation accuracy is not very likely due to wide popularity of the problem. When comparing oracle center and oracle offsets we observe that the latter one brings significantly larger improvements: 3 PQ and 10 AP points over the regular model. In early experiments most of the offset errors were located at instance boundaries, so we introduced the boundary aware offset loss [26, 11].

**Table 3. Evaluation of models with different oracle components. Labels +GT X denote models which use groundtruth information for the prediction X. Note that c. & o. denotes centers and offsets.**

Model	PQ	SQ	RQ	AP	mIoU
PSN-RN18	55.9	79.5	68.9	26.1	77.2
+ GT semseg	76.2	91.0	82.5	39.6	100.0
+ GT centers	56.9	79.5	70.1	22.9	77.2
+ GT offsets	59.1	83.0	70.4	36.8	77.2
+ GT c. & o.	61.6	83.3	73.2	38.2	77.2

**Table 2. Comparison of spatial pyramid pooling with pyramidal fusion in conjunction with PSN-RN18 on Cityscapes val. Both PYRx1 and SPP models operate on single resolution and hence can not exploit pyramidal fusion. The SPP model applies spatial pyramid pooling [12, 25] to  $32 \times$  subsampled abstract features at the far end of the backbone.**

Method	PQ	SQ	RQ	AP	mIoU	FPS
single-scale	51.7	78.4	64.3	18.7	71.2	34.5
SPP	53.5	78.8	66.3	22.4	75.1	32.2
PYRx2	54.9	79.2	67.8	23.3	76.1	30.3
PYRx3	<b>55.9</b>	<b>79.5</b>	<b>68.9</b>	<b>26.1</b>	<b>77.2</b>	28.6

Table 4 explores the influence of the boundary-aware offset loss 1 to the PSN-18 accuracy. Note that we reduce the overall weight of the offset loss to  $\lambda_{BAOL} = 0.025$  when we use the boundary aware formulation (1) because it increases the loss magnitude in pixels near instance boundaries. We observe that boundary aware offset loss brings noticeable improvements across all metrics. The largest improvement is in instance seg-

mentation performance which increases for 1.8pp AP.

**Table 4. Validation of boundary-aware offset loss for the PSN-RN18 PYR<sub>x</sub>3 model on Cityscapes val.**

Offset loss	PQ	SQ	RQ	AP	mIoU
L1	55.4	79.3	68.4	24.3	76.4
L1-BAL	<b>55.9</b>	<b>79.5</b>	<b>68.9</b>	<b>26.1</b>	<b>77.2</b>

### 3.2. Inference speed after TensorRT optimization

Figure 3 evaluates speed of our optimized models across different input resolutions. All models have been run from Python within the TensorRT execution engine. We have used TensorRT to optimize the same model for two graphics cards and two precisions (FP16 and FP32). Note however that these optimizations involve only the network inference, and not the postprocessing step as we explain later.

Interestingly, FP16 brings almost  $2\times$  improvement across all experiments, although RTX3090 declares the same peak performance for FP16 and FP32. This suggests that it is likely that our performance bottleneck corresponds to memory bandwidth rather than computing power.

We start the clock when an image is synchronized in CUDA memory and stop it when the postprocessing is completed. We implement the postprocessing using cupy. We believe that the runtime could be even faster if postprocessing were also executed by TensorRT. We capture realistic post-processing times by expressing all datapoints as average inference speed over all images from Cityscapes val. The figure shows that our model achieves realtime inference speed even on high resolution 2MPx images. Our PSN-RN18 model achieves more than 100 FPS on 1MPx resolution with FP16 RTX3090.

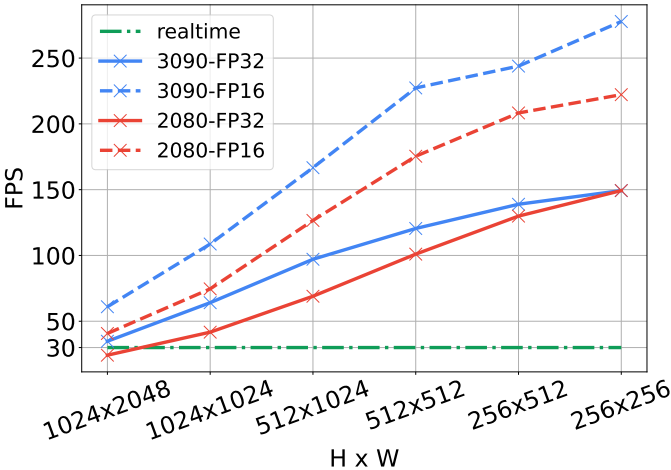


**Fig. 3. Inference speed of a three-level PSN-RN18 across different input resolutions for two graphics cards and two precisions. All configurations involve the same model after optimizing it with Tensor RT. All datapoints are averaged over all images from Cityscapes val in order to account for the dependence of the postprocessing time on scene complexity.**

### 3.3. Qualitative experiments

Figure 4 shows qualitative results on two scenes from Cityscapes val. The rows show: input image, semantic seg-

mentation, centers heatmap, offset directions and the panoptic segmentation. Offset directions are color coded according to the convention established by the previous work in optical flow [27]. Panoptic maps designate instances with different shades of the color of the corresponding class. Column 1 shows a scene with cars parked on both sides of the road. We observe that our model succeeds to correctly differentiate all distinct instances. Edges between the instances are sharp and accurate in the offset map. Column 2 shows a scene with a large truck on the left. Semantic segmentation mistakenly recognizes a blob of pixels in the bottom-left as class bus instead as class truck. However, the panoptic map shows that the postprocessing step succeeds to correct the mistake since the correct predictions outvoted the incorrect ones. Hence, the instance segmentation of the truck was completely correct.

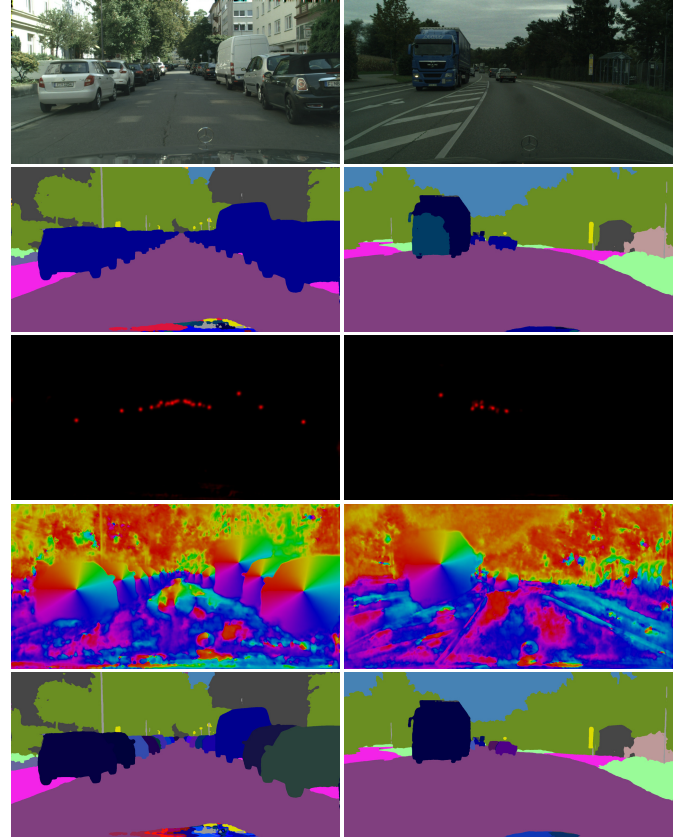


**Fig. 4. Qualitative results on two scenes from Cityscapes val. Rows show: input image, semantic segmentation, centers heatmap, offset directions, and panoptic segmentation.**

### 3.4. COCO

COCO dataset [16] contains digital photographs collected by Flickr users. Images are annotated with 133 semantic categories [28]. The standard split proposes 118K images for training, 5K for validation and 20K for testing. We train for 200K iterations with ADAM optimizer on  $640 \times 640$  crops with batch size 48. This can be carried out on 2 GPU(s) each with 20 GiB of RAM. We set learning rate to  $4 \cdot 10^{-4}$  and use polynomial rate decay.

Table 5 presents our results on COCO val. We compare our performance with previous work by evaluating  $640 \times 640$  crops.



We achieve the best accuracy among the methods with real-time execution speed. Although designed for large resolution images, pyramidal fusion performs competitively even on COCO images with median resolution of  $640 \times 480$  pixels. Figure 5 shows qualitative results on COCO val.

**Table 5. Panoptic segmentation performance of pyramidal fusion models on COCO val. We do not optimize our models with TensorRT in order to ensure a fair comparison with the previous work.**

Model	PQ	PQ <sub>th</sub>	PQ <sub>st</sub>	FPS	GPU
PanopticFPN-RN101 [2]	40.3	47.5	29.5	-	-
DeeperLab-WMNv2 [4]	28.1	30.8	24.1	12.0	V100
Max-Deeplab-S [22]	48.4	53.0	41.5	14.9	V100
RTPS-RN50 [7]	37.1	41.0	31.3	15.9	V100
PanopticFCN-RN50 [21]	42.8	47.9	35.1	16.8	V100
PDL-MNV3 [3]	30.0	-	-	26.3	V100
PSN-RN18 (ours)	30.5	32.1	28.1	64.5	RTX3090
PSN-DN121 (ours)	33.6	35.7	30.5	14.7	RTX3090

### 3.5. Mapillary Vistas

Mapillary Vistas dataset [17] collects high resolution images of road driving scenes taken under wide variety of conditions. It contains 18K train, 2K val and 5K test images densely labeled with 65 semantic categories. We train for 200K iterations with ADAM optimizer on  $1024 \times 1024$  crops and batch size 16. We use image and crop sampling which favors rare classes. During evaluation we resize the input image so that the longer side is equal to 2048 pixels while maintaining the original aspect ratio. Similarly, during training we randomly resize the input image so that the mean resolution is equal to the one in the evaluation.

Table 6 presents our results on Vistas val. Our model achieves comparable accuracy w.r.t. literature, while being much faster. These models are slower than their Cityscapes counterparts from Table 1 for two reasons. First, average resolution of Vistas images in our training and evaluation experiments is  $1536 \times 2048$  while the Cityscapes resolution is  $1024 \times 2048$ . Second, these models also have slower classification and postprocessing steps due to a larger number of classes and instances. Figure 6 shows qualitative results on two scenes.

**Table 6. Panoptic segmentation performance of pyramidal fusion model on Mapillary Vistas val. We report average FPS over all validation images.**

Model	PQ	mIoU	FPS	GPU
DeeperLab-WMNv2 [4]	22.4	/	3.3	V100
PDL-MNV3 [3]	28.8	/	6.8	V100
PDL-RN50 [3]	33.3	/	3.5	V100
PSN-RN18 (ours)	28.6	47.8	17.0	RTX3090

## 4. Conclusion

We have proposed an adaptation of the pyramidal SwiftNet architecture for the panoptic segmentation task. Our work indicates clear advantages of multi-scale feature extraction, pyramidal fusion and boundary-aware regularization to the panoptic performance. Experiments with oracle components suggest

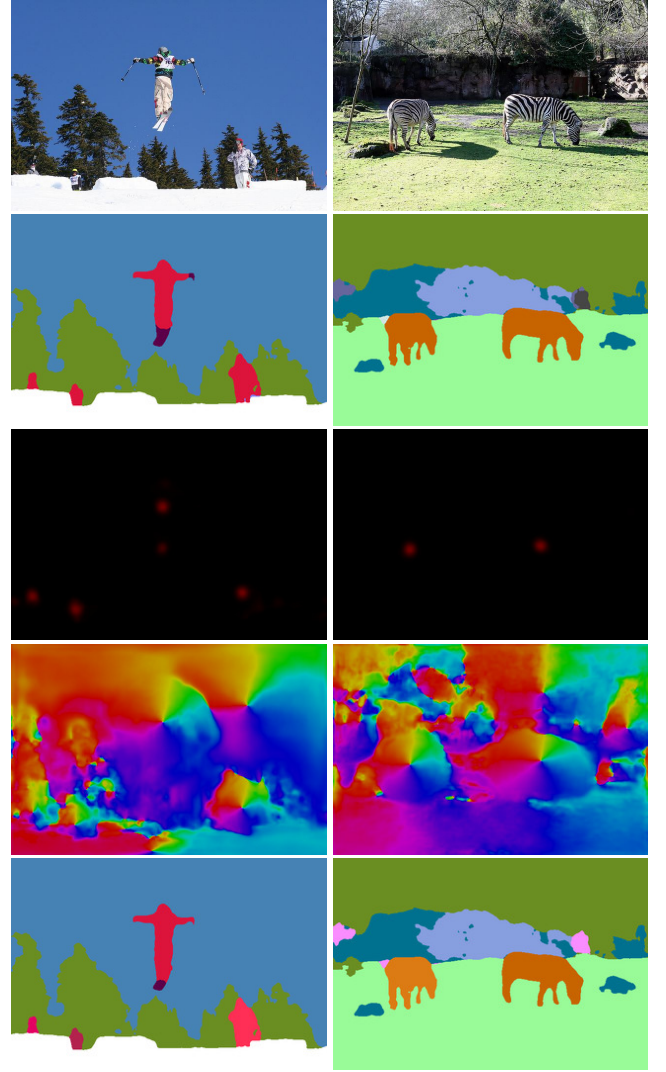


**Fig. 5. Qualitative results on two scenes from COCO val. Rows show: input image, semantic segmentation, centers heatmap, offset directions, and panoptic segmentation.**

that semantic segmentation represents a critical ingredient of panoptic performance. Panoptic SwiftNet-RN18 achieves state-of-the-art generalization performance on Cityscapes as well as competitive performance on Vistas and COCO among all models aiming at real-time inference. Source code will be publicly available upon acceptance.

## Acknowledgments

This work has been funded by Rimac Technology. This work has also been supported by the Croatian Science Foundation under the grant ADEPT and European Regional Development Fund under the grant KK.01.1.1.01.0009 DATACROSS.

## References

- [1] A. Kirillov, K. He, R. Girshick, C. Rother, P. Dollár, Panoptic segmentation, in: Proceedings of the IEEE/CVF Conference on Computer Vision and Pattern Recognition, 2019, pp. 9404–9413.

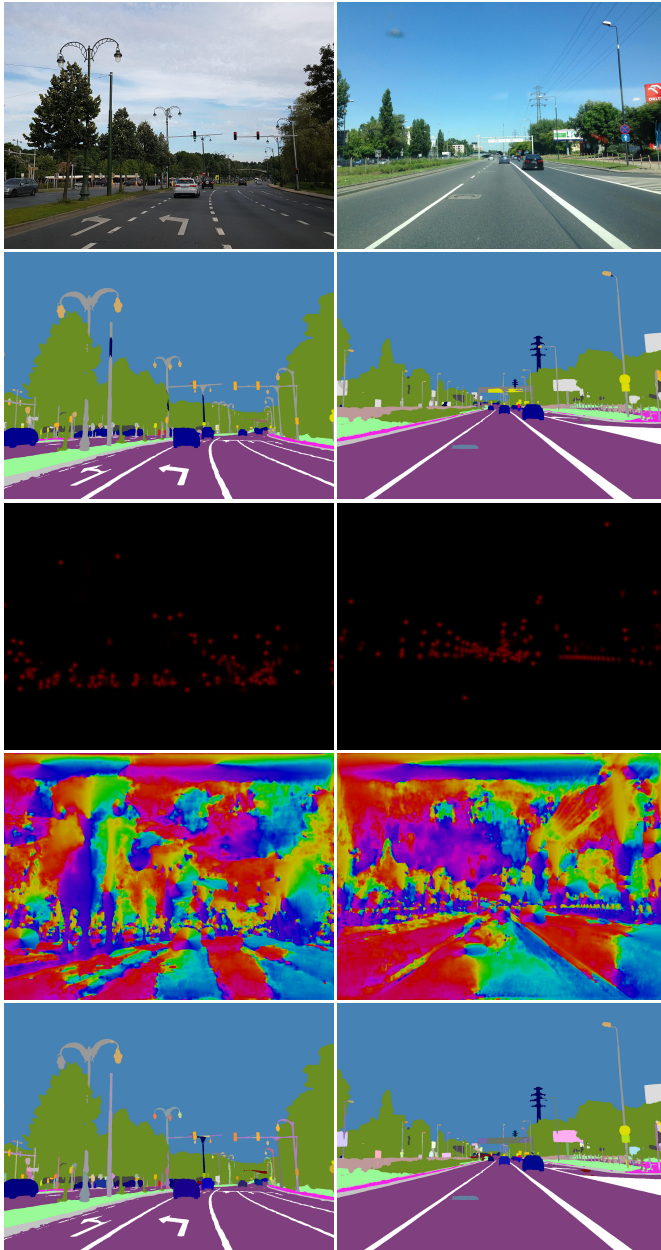


**Fig. 6. Qualitative results on two scenes from Mapillary Vistas val. Rows show: input image, semantic segmentation, centers heatmap, offset directions, and panoptic segmentation.**

- [2] A. Kirillov, R. Girshick, K. He, P. Dollár, Panoptic feature pyramid networks, in: *Proceedings of the IEEE/CVF Conference on Computer Vision and Pattern Recognition*, 2019, pp. 6399–6408.
- [3] B. Cheng, M. D. Collins, Y. Zhu, T. Liu, T. S. Huang, H. Adam, L.-C. Chen, Panoptic-deeplab: A simple, strong, and fast baseline for bottom-up panoptic segmentation, in: *Proceedings of the IEEE/CVF Conference on Computer Vision and Pattern Recognition (CVPR)*, 2020.
- [4] T.-J. Yang, M. D. Collins, Y. Zhu, J.-J. Hwang, T. Liu, X. Zhang, V. Sze, G. Papandreou, L.-C. Chen, Deeplab: Single-shot image parser, *arXiv preprint arXiv:1902.05093* (2019).
- [5] L. Porzi, S. R. Buló, A. Colovic, P. Kotschieder, Seamless scene segmentation, in: *Proceedings of the IEEE/CVF Conference on Computer Vision and Pattern Recognition (CVPR)*, 2019.
- [6] H. Wang, Y. Zhu, B. Green, H. Adam, A. Yuille, L.-C. Chen, Axial-deeplab: Stand-alone axial-attention for panoptic segmentation, in: *European Conference on Computer Vision*, Springer, 2020, pp. 108–126.
- [7] R. Hou, J. Li, A. Bhargava, A. Raventos, V. Guizilini, C. Fang, J. Lynch, A. Gaidon, Real-time panoptic segmentation from dense detections, in: *Proceedings of the IEEE/CVF Conference on Computer Vision and Pattern Recognition (CVPR)*, 2020.
- [8] Y. Xiong, R. Liao, H. Zhao, R. Hu, M. Bai, E. Yumer, R. Urtasun, Upsnet: A unified panoptic segmentation network, in: *Proceedings of the IEEE/CVF Conference on Computer Vision and Pattern Recognition*, 2019, pp. 8818–8826.
- [9] M. Oršić, I. Kreso, P. Bevandic, S. Šegvić, In defense of pre-trained imagenet architectures for real-time semantic segmentation of road-driving images, in: *Proceedings of the IEEE/CVF Conference on Computer Vision and Pattern Recognition (CVPR)*, 2019.
- [10] I. Krešo, D. Čaušević, J. Krapac, S. Šegvić, Convolutional scale invariance for semantic segmentation, in: *German conference on pattern recognition*, Springer, 2016, pp. 64–75.
- [11] M. Oršić, S. Šegvić, Efficient semantic segmentation with pyramidal fusion, *Pattern Recognition* 110 (2021) 107611.
- [12] H. Zhao, J. Shi, X. Qi, X. Wang, J. Jia, Pyramid scene parsing network, in: *Proceedings of the IEEE conference on computer vision and pattern recognition*, 2017, pp. 2881–2890.
- [13] J. Yao, S. Fidler, R. Urtasun, Describing the scene as a whole: Joint object detection, scene classification and semantic segmentation, in: *2012 IEEE conference on computer vision and pattern recognition*, IEEE, 2012, pp. 702–709.
- [14] N. Dvornik, K. Shmelkov, J. Mairal, C. Schmid, Blitznet: A real-time deep network for scene understanding, in: *Proceedings of the IEEE international conference on computer vision*, 2017, pp. 4154–4162.
- [15] M. Cordts, M. Omran, S. Ramos, T. Rehfeld, M. Enzweiler, R. Benenson, U. Franke, S. Roth, B. Schiele, The cityscapes dataset for semantic urban scene understanding, in: *Proceedings of the IEEE Conference on Computer Vision and Pattern Recognition (CVPR)*, 2016.
- [16] T.-Y. Lin, M. Maire, S. Belongie, J. Hays, P. Perona, D. Ramanan, P. Dollár, C. L. Zitnick, Microsoft coco: Common objects in context, in: *European conference on computer vision*, Springer, 2014, pp. 740–755.
- [17] G. Neuhold, T. Ollmann, S. Rota Buló, P. Kotschieder, The mapillary vistas dataset for semantic understanding of street scenes, in: *Proceedings of the IEEE International Conference on Computer Vision*, 2017, pp. 4990–4999.
- [18] K. He, G. Gkioxari, P. Dollár, R. Girshick, Mask r-cnn, in: *Proceedings of the IEEE international conference on computer vision*, 2017, pp. 2961–2969.
- [19] R. Mohan, A. Valada, Efficienttps: Efficient panoptic segmentation, *International Journal of Computer Vision* 129 (5) (2021) 1551–1579.
- [20] L.-C. Chen, Y. Zhu, G. Papandreou, F. Schroff, H. Adam, Encoder-decoder with atrous separable convolution for semantic image segmentation, in: *ECCV*, 2018.
- [21] Y. Li, H. Zhao, X. Qi, L. Wang, Z. Li, J. Sun, J. Jia, Fully convolutional networks for panoptic segmentation, in: *Proceedings of the IEEE/CVF Conference on Computer Vision and Pattern Recognition (CVPR)*, 2021, pp. 214–223.
- [22] H. Wang, Y. Zhu, H. Adam, A. Yuille, L.-C. Chen, Max-deeplab: End-to-end panoptic segmentation with mask transformers, in: *Proceedings of the IEEE/CVF Conference on Computer Vision and Pattern Recognition (CVPR)*, 2021, pp. 5463–5474.
- [23] K. He, X. Zhang, S. Ren, J. Sun, Deep residual learning for image recognition, in: *Proceedings of the IEEE Conference on Computer Vision and Pattern Recognition (CVPR)*, 2016.
- [24] G. Huang, Z. Liu, L. Van Der Maaten, K. Q. Weinberger, Densely connected convolutional networks, in: *Proceedings of the IEEE conference on computer vision and pattern recognition*, 2017, pp. 4700–4708.
- [25] I. Krešo, J. Krapac, S. Šegvić, Efficient ladder-style densenets for semantic segmentation of large images, *IEEE Transactions on Intelligent Transportation Systems* 22 (8) (2020) 4951–4961.
- [26] M. Zhen, J. Wang, L. Zhou, T. Fang, L. Quan, Learning fully dense neural networks for image semantic segmentation, in: *Proceedings of the AAAI Conference on Artificial Intelligence*, Vol. 33, 2019, pp. 9283–9290.
- [27] S. Baker, D. Scharstein, J. Lewis, S. Roth, M. J. Black, R. Szeliski, A database and evaluation methodology for optical flow, *International journal of computer vision* 92 (1) (2011) 1–31.
- [28] H. Caesar, J. Uijlings, V. Ferrari, Coco-stuff: Thing and stuff classes in context, in: *Proceedings of the IEEE conference on computer vision and pattern recognition*, 2018, pp. 1209–1218.